A Comparison of Fault Behaviour of Bipolar vs. Unipolar LVDC Grids

L. Hallemans*†, G. Govaerts*†, S. Ravyts*†, M. M. Alam ‡†, P. Van Tichelen‡†, J. Driesen *†
*KU Leuven, Dept. of Electrical Engineering, div. Electa, Kasteelpark Arenberg 10 bus 2440, 3001 Leuven, Belgium
†EnergyVille, Thor Park 8301, 3600 Genk, Belgium
‡VITO, Boeretang 200, 2400 Mol, Belgium

***Abstract*—Over the past years, there has been an increasing scientific interest in LVDC microgrids as an alternative for AC microgrids. Ongoing research mainly focusses on the two-wire unipolar architecture and, although the bipolar structure may offer several advantages, it is often regarded as just a double version of its unipolar equivalent. This paper compares the behaviour of unipolar and bipolar LVDC microgrids under fault conditions to demonstrate that this generalisation is not always valid. The differences in the fault behaviour of a unipolar and bipolar structure are first introduced by calculating the first fault transient in a fundamental example of both structures. Subsequently, PSCAD simulations of faults in a unipolar and bipolar LVDC microgrid are compared to demonstrate the differences between the two structures in a realistic LVDC microgrid context. These simulations are then applied to show the potential impact of generalising conclusions from one structure to the other on the protection algorithm of the LVDC grid. It is shown that a protection algorithm designed for one of the structures does not necessarily work in the other structure. Finally, an experimental validation of the differences observed regarding the fault behaviour of both structures is presented.**

I. Introduction

In recent years, scientific interest in LVDC grids has been growing, driven mainly by their higher efficiency, transmission capacity and compatibility compared to traditional LVAC grids [1], [2]. A three-wire, bipolar LVDC grid architecture has the potential to further enhance the advantages of an LVDC grid: It allows increase the power transfer capability and reduce conduction losses compared to a unipolar equivalent, while also potentially increasing reliability [3]–[5]. Furthermore, a bipolar grid offers two voltage levels, allowing to connect load-side converters to the most appropriate voltage [6]. Despite these advantages, most current research on LVDC fault behaviour and protection focusses mainly on the unipolar LVDC grid architecture [7]–[13]. If the bipolar structure is considered, often no distinction is made between unipolar and bipolar short circuit fault behaviour [7], [8] or research is only evaluated for one of the two structures [13], [14]. This paper will compare the fault behaviour of a bipolar LVDC grid with its unipolar equivalent to demonstrate that a bipolar LVDC grid cannot always simply be regarded as a 'double' unipolar grid. To this end, Section II introduces the differences between the unipolar and bipolar structure w.r.t. fault behaviour using a fundamental mathematical example. Subsequently, Section III presents PSCAD simulations of a unipolar and bipolar LVDC microgrid in fault conditions to illustrate these differences and confirm the trends observed in Section II in a realistic LVDC microgrid. In Section IV, the potential impact of these differences on protection algorithms designed for one of the two structures is investigated. Section V presents the results of a fault experiment in a scaled, single-branch unipolar and bipolar LVDC lab setup to validate the differences and trends observed in the calculations and simulations. Finally, Section VI summarises the conclusions of the paper.

II. Fault behaviour difference

In order to introduce the differences in the fault behaviour of unipolar and bipolar LVDC microgrids, this section compares the first fault current peak caused by the discharge of the DC bus capacitance in both structures in the simplified example of Figure 1, applying the approximation described in [15], [16]. The figure shows the simplified unipolar and bipolar structure of a small LVDC grid connecting a DC load to a DC source protected by circuit breakers. The capacitive discharge upon a fault with $R_f = 40\,\mathrm{m\Omega}$ close to the load is calculated based on the mesh equations (1) to (2) for the unipolar and (3) to (5) for the bipolar structure, with $L_a = 11.8\,\mu\mathrm{H}$, $L_b = 0.24\,\mu\mathrm{H}$, $R_a = 24.4\,\mathrm{m\Omega}$, $R_b = 0.49\,\mathrm{m\Omega}$, $C = 1\,\mathrm{mF}$, $V_{dc} = 375\,\mathrm{V}$.

$$4L_a\frac{d^2i_1}{dt^2} + 4R_a\frac{di_1}{dt} + R_f\left(\frac{di_1}{dt} + \frac{di_2}{dt}\right) + \frac{1}{C}i_1(t) = 0 \quad (1)$$

$$2L_b\frac{d^2i_2}{dt^2} + 2R_b\frac{di_2}{dt} + R_f\left(\frac{di_1}{dt} + \frac{di_2}{dt}\right) + \frac{1}{C}i_2(t) = 0 \quad (2)$$

$$\begin{aligned}4L_a\frac{d^2i_1}{dt^2} - 2L_a\frac{d^2i_3}{dt^2} + 4R_a\frac{di_1}{dt} - 2R_a\frac{di_3}{dt} + R_f\frac{di_1}{dt}\\ +R_f\frac{di_2}{dt} + \frac{1}{C}i_1(t) = 0\end{aligned} \quad (3)$$

$$\begin{aligned}2L_b\frac{d^2i_2}{dt^2} + L_b\frac{d^2i_3}{dt^2} + 2R_b\frac{di_2}{dt} + R_b\frac{di_3}{dt} + R_f\frac{di_1}{dt}\\ +R_f\frac{di_2}{dt} + \frac{1}{C}i_2(t) = 0\end{aligned} \quad (4)$$

$$\begin{aligned}-2L_a\frac{d^2i_1}{dt^2} + L_b\frac{d^2i_2}{dt} + (4L_a + 2L_b)\frac{d^2i_3}{dt^2} - 2R_a\frac{di_1}{dt}\\ +R_b\frac{di_2}{dt} + (4R_a + 2R_b)\frac{di_3}{dt} + \frac{2}{C}i_3(t) = 0\end{aligned} \quad (5)$$

As can be seen in Figure 1, there is an additional path (i_3) for the current to flow in the bipolar structure through the midpoint and negative conductor, which is not present in the unipolar structure. Figure 2a shows the resulting fault current after solving equations (1) to (5), which coincide rather well, especially during the first fault peak. Figure 2b, on the other hand, shows

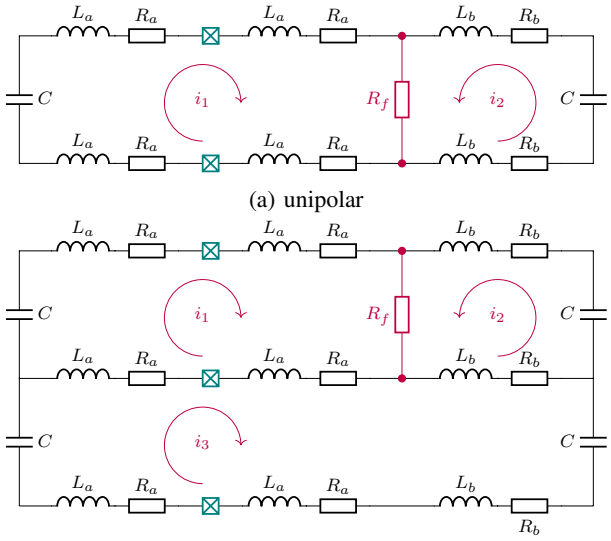

(a) unipolar

(b) bipolar

Fig. 1: Fundamental example of uni- and bipolar fault behaviour

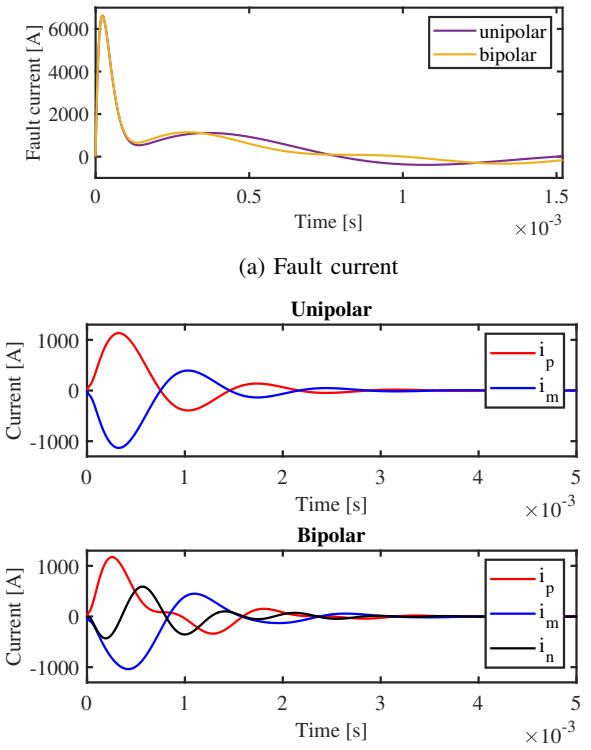

(a) Fault current

(b) Protection device current

Fig. 2: Calculation result of the uni- and bipolar fundamental example

the current measured by the circuit breakers during the fault in both structures. The bipolar measurement indeed shows a (comparatively small) current flowing through the negative conductor (in black) and consequently, the positive (red) and midpoint (blue) current measurements in the bipolar structure differ from the unipolar measurements. Specifically, the peak of the fault current in the bipolar positive pole is slightly higher than the unipolar peak and is reached significantly faster, while the bipolar midpoint current transient is slowed down compared to the unipolar midpoint current. These differences indicate that, although the fault current flowing through the fault in the unipolar and bipolar structure is approximately equal, there may be a substantial difference between the unipolar and bipolar currents measured at other locations in the grid.

III. PSCAD SIMULATIONS

The aim of this section is to investigate how the different fault behaviour of unipolar and bipolar structures described in Section II may impact real LVDC microgrids. To this end, a unipolar and a bipolar version of the multibranch LVDC microgrid shown in Figure 3 have been modelled in PSCAD. The microgrid is connected to the AC grid through an AC/DC full bridge converter, the DC loads are connected through DC/DC buck converters. The AC/DC converter is rated for $I^1_{nom} = 100\,\text{A}$, while the DC/DC load converters are rated for $I^2_{nom} = 10\,\text{A}$. Figure 4 depicts the technical model of the bipolar structure, including the converter and cable models. Table I gives an overview of the cable and converter characteristics. As clear from Figure 3a, the unipolar model can be derived from the bipolar model by using a two-wire structure instead of three wires and connecting unipolar AC/DC and DC/DC converters instead of bipolar (parallelised) converters.

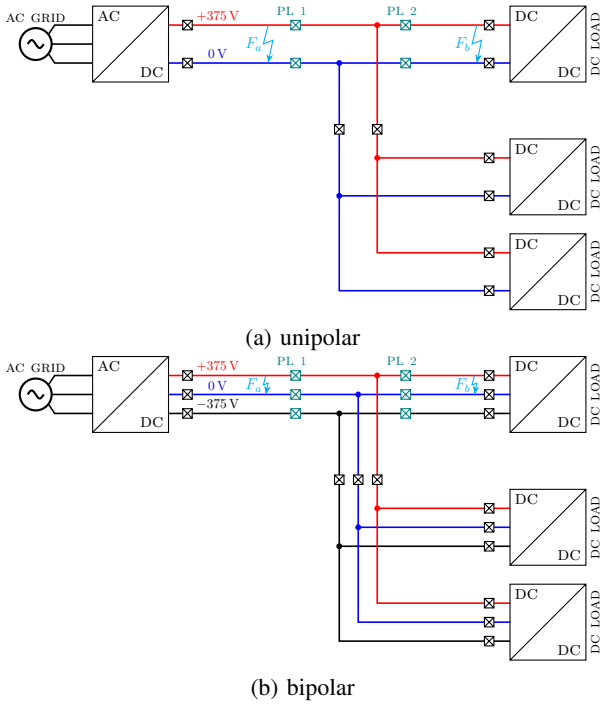

(a) unipolar

(b) bipolar

Fig. 3: Example of uni- and bipolar LVDC microgrid

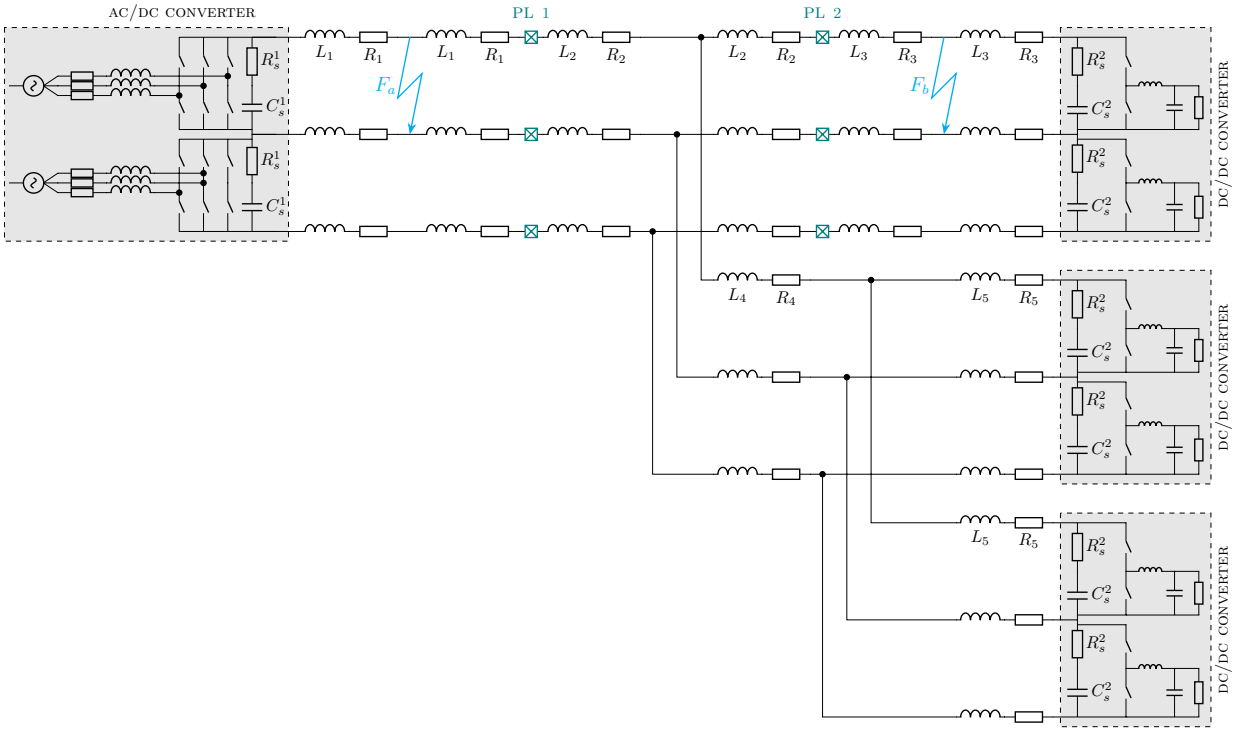

Fig. 4: Technical overview of the bipolar grid structure

TABLE I: Microgrid characteristics

CABLE INDUCTANCE		CABLE RESISTANCE	
L_1	5.9 µH	R_1	12.2 mΩ
L_2	0.47 µH	R_2	0.98 mΩ
L_3	5.9 µH	R_3	12.2 mΩ
L_4	6.14 µH	R_4	12.69 mΩ
L_5	7.26 µH	R_5	31.1 mΩ
AC/DC CONVERTER		DC/DC CONVERTER	
C_s^1	1 mF	C_s^2	0.1 mF
R_s^1	1 mΩ	R_s^2	1 mΩ
I_{nom}^1	100 A	I_{nom}^2	10 A

The unipolar cable and grid characteristics are identical to those of the bipolar structure. The protection devices that are of interest for this paper have been marked Protection Location (PL) 1 and 2 in Figures 3 and 4. For clarity, the other protection devices are not shown in the detailed structure of Figure 4. A short circuit fault protection strategy designed for the bipolar LVDC grid, which relies on a communicationless protection algorithm based on a combination of overcurrent and current derivative detection, is implemented on the circuit breakers in both grids. To compare the fault behaviour of the unipolar and bipolar structure, fault *a* and fault *b*, as shown in Figures 3a and 3b, are simulated in PSCAD with the protection algorithm disabled.

A. *Fault a*

Fault *a* represents a fault close to the AC/DC converter, which is the source of the microgrid. Figure 5a shows the fault current flowing due to a short circuit fault with $R_f = 40\,\mathrm{m\Omega}$ at fault location *a* in the unipolar (purple) and bipolar (yellow) microgrid. The fault current consists of a rapid and high first fault current peak, caused by the discharge of the capacitors in the grid, and the steady state fault current fed mainly by the AC grid. It is clear that the fault currents in the unipolar and bipolar structure are nearly identical during the first fault transient, which corresponds to the conclusions from Section II. Because it is the most important protection device to react in case of fault *a*, the current and the derivative of the positive pole current measured by PL 1 during the fault are shown for both structures in Figures 5b and 5c, respectively. The results show that the current and derivative measurements at PL 1 due to fault *a* approximately coincide as well.

B. *Fault b*

Fault *b* represents a fault close to one of the DC/DC converters, which act as a load. Figure 6a shows the fault current at fault location *b* in the unipolar and bipolar grid. The figure shows that the fault currents are again nearly identical during the first fault current peak, but start to deviate slightly after the first peak. Figures 6b and 6c, on the other hand, show the current (6b) and positive pole current derivative (6c) measured at PL 2, which is the most important protection location for this fault. It is clear that the measurements by the responsible protection device in the unipolar and bipolar grid differ more in this case than in case of fault *a*. Similar to the findings of Section II, the bipolar positive pole current initially increases faster than in the unipolar positive pole, while the waveform in the bipolar midpoint conductor is slowed down

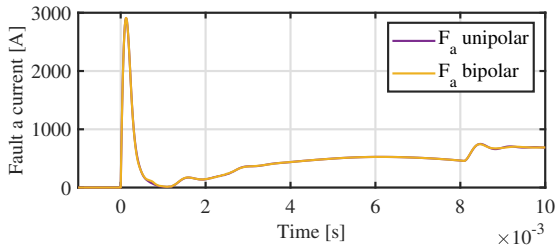

(a) Fault *a* current

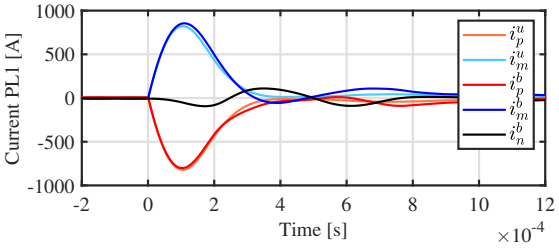

(b) PL 1 current

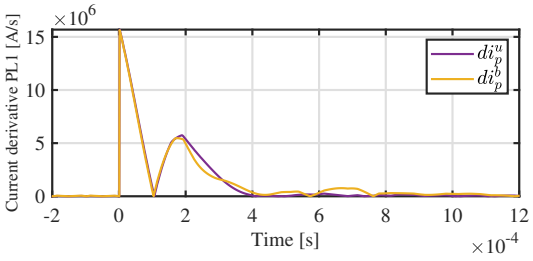

(c) PL 1 positive pole current derivative

Fig. 5: PSCAD simulation results of fault *a*

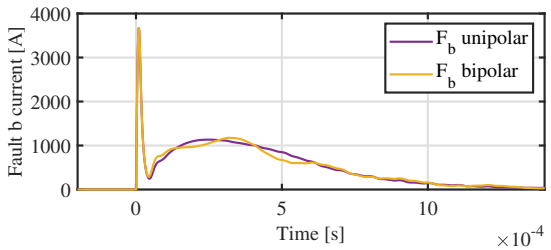

(a) Fault *b* current

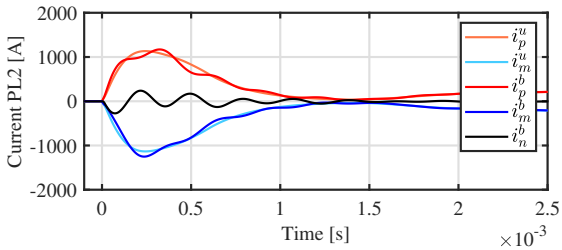

(b) PL2 current

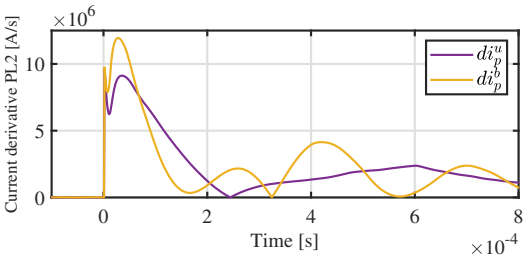

(c) PL 2 positive pole current derivative

Fig. 6: PSCAD simulation results of fault *b*

compared to its unipolar equivalent. As a result, the size of the current derivative at PL 2 during the first fault transient is significantly lower in the unipolar structure than in the bipolar structure, as illustrated by Figure 6c. As will be explained in Section IV, this may pose a problem for a protection algorithm which is designed while considering only one of the two structures.

These simulation results show same trends as encountered in the mathematical example of Section II for both fault *a* and *b*, although it is barely noticeable in case of fault *a* because the unipolar and bipolar waveforms are very similar. However, the differences between the unipolar and bipolar simulation are smaller than in the simplified example. It is also clear that for different fault situations and measurement locations, the differences in unipolar and bipolar fault behaviour may vary: For fault *a* there is only a very small difference between the unipolar and bipolar measurements at PL 1, while for fault *b* the difference measured at PL 2 is substantially larger.

IV. Effects on Protection Algorithm

As mentioned in Section III, a protection strategy has been designed a priori for the bipolar LVDC grid structure of Figure 3b, without taking the unipolar structure into account, to illustrate the issues that may arise when generalising conclusions on the fault behaviour from one architecture to the other. It is comprised of a local, measurement-based protection algorithm that is installed on each of the protection devices in the grid without using communication, such as the examples presented in [8], [9], [11], [12]. An overcurrent and current derivative limit for the fault detection were determined based upon a characterisation of the fault behaviour of the bipolar structure. Specifically, the limits $i \geq 500\,\mathrm{A}$ and $\frac{di}{dt} \geq 1 \times 10^7\,\mathrm{A\,s^{-1}}$ were found to be sufficiently sensitive and selective to protect against faults in this bipolar microgrid. To illustrate the potential problems when a bipolar LVDC grid is viewed simply as a 'double' unipolar grid w.r.t protection, the reaction of the protection algorithm to fault *a* and *b* in both structures is compared in this section.

A. Fault a

Figure 7 shows the response of the protection algorithm to a PSCAD simulation of fault *a* in the unipolar and bipolar structure. As discussed in Section III-A, the fault transient as a result of fault *a* is very similar in both structures and hence, as expected the figure demonstrates that the algorithm detects the fault in both cases and sends a tripping signal to PL 1 after 39 µs. In other words, these simulation results show that, in case of fault situation *a*, a protection algorithm designed

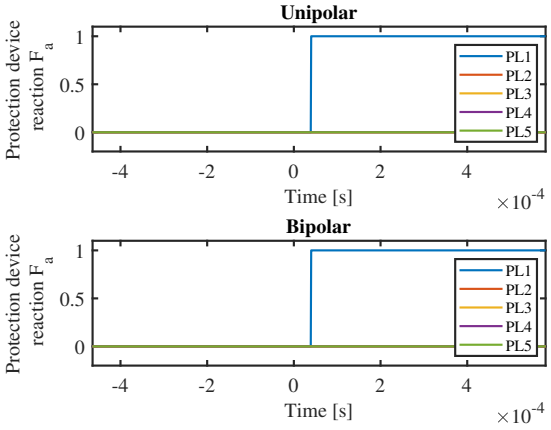

Fig. 7: Protection algorithm response to fault *a*

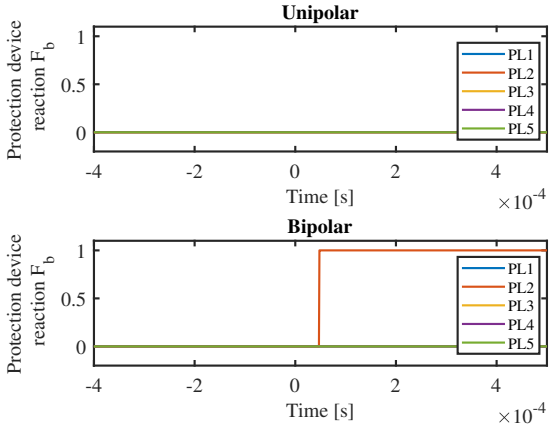

Fig. 8: Protection algorithm response to fault *b*

and validated for the bipolar grid will also be able to protect against fault *a* in the unipolar grid.

B. Fault b

As explained in Section III-B, there is a significant difference between the fault transients measured in the unipolar and bipolar structure at PL 2, which is the primary protection device that should protect the rest of the grid against fault *b*, especially regarding the current derivative measurement. It can be seen in Figure 6c that, although a current derivative threshold of $\frac{di}{dt} \geq 1 \times 10^7\,\mathrm{A\,s^{-1}}$ worked well for the bipolar structure, it is not crossed in case of fault *b* in the unipolar structure. Figures 8 and 9 show the effect of this problem in a PSCAD simulation of fault *b* in both structures with the protection algorithm enabled. Figure 8 shows the response of the protection algorithm to fault *b*, demonstrating that the protection algorithm detects the short circuit and trips PL 2 after approximately $47\,\mu\mathrm{s}$ in the bipolar grid, but that the fault remains undetected in the unipolar structure. Furthermore, Figure 9a shows that, although the fault current in both grids is nearly identical, only the bipolar fault current is cut off by the tripping of PL 2. As a result, there is only a small disturbance in the DC bus voltage in the bipolar LVDC grid, which is able to remain operational by isolating the faulty branch, as shown by Figure 9b, while the unipolar DC bus voltage completely collapses. It can be concluded that in case of fault situation *b* a protection algorithm designed and validated for the bipolar grid is not capable of protecting the grid in an equivalent unipolar grid structure. This also implies that, in case one of the poles of the bipolar grids is isolated, for instance because of a prior fault, and the grid operation is continued in a unipolar configuration, its protection algorithm may have problems detecting the faults it was designed for.

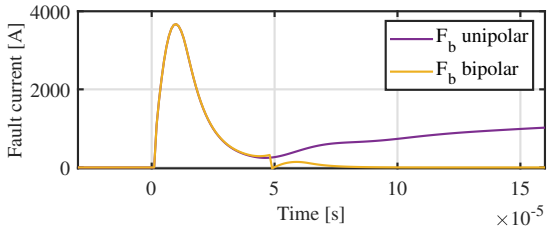

(a) Fault current

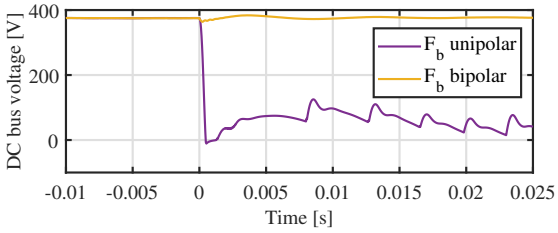

(b) DC bus voltage

Fig. 9: Fault transient and voltage fault *b* with protection algorithm enabled

V. Experiments

To validate the observations of the previous sections, the scaled, single-branch unipolar and bipolar LVDC lab setup shown in Figure 10 was built for fault experiments. The setup consists of four Delta Elektronika units, of which two unidirectional units (SM 660-AR-11) act as the bipolar source and two bidirectional units (SM 500-CP-90) act as the bipolar load of the grid. The source and load are connected through approximately $100\,\mathrm{m}$ cable and extra DC bus capacitance was added to the relatively low source capacitance. The experiments were performed at $\pm 200\,\mathrm{V}$. Figure 11 shows the resulting current measurement at the locations depicted in Figure 10 for the unipolar and bipolar short circuit experiment. The unipolar experiment was performed by disconnecting the negative conductor and the corresponding source and load unit. The measurements confirms the observations presented in paragraphs II and III: Compared to the unipolar measured current, the bipolar positive pole current has a slightly higher peak, which is reached faster, while the current transient flowing through the midpoint conductor is slowed down.

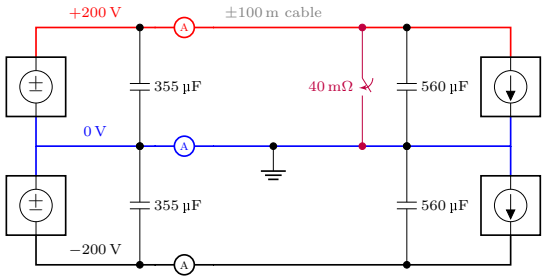

Fig. 10: Experimental lab setup

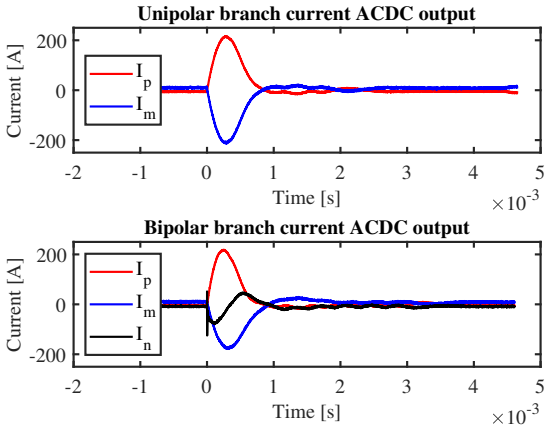

Fig. 11: Current measurement during the fault experiment

VI. Conclusion

The aim of this paper was to compare the fault behaviour of a unipolar and bipolar LVDC microgrid with the same specifications and grid characteristics, in order to demonstrate the potential problems when regarding a bipolar LVDC grid simply as a double version of its unipolar equivalent et vice versa. The differences between the fault behaviour in both structures was introduced by calculating the first short circuit current transient in a fundamental mathematical unipolar and bipolar example. The resulting short circuit current waveforms showed that, due to the additional path for the current in the bipolar structure, the bipolar positive and midpoint currents flowing due to the short circuit differed from the currents flowing in the unipolar structure. Specifically, the current transient measured in the bipolar positive pole was higher and faster than its unipolar equivalent, while the transient in the bipolar midpoint conductor was slowed down. Subsequently, PSCAD simulations of a short circuit at different locations in a realistic LVDC microgrid were presented. When comparing the simulations of the unipolar and bipolar microgrid in fault conditions, the same trends were observed as in the mathematical example. Furthermore, it was concluded that the extent to which the unipolar and bipolar currents differ depends on the fault location and the measurement location. Based on the simulations, the potential effect of these differences on a protection algorithm were investigated. It was found that a protection algorithm designed and validated for one of both grid structures will not necessarily work in the other structure. In other words, care should be taken when generalising conclusions on the fault behaviour from one structure to the other, especially concerning protection algorithms that are based on local measurements. Finally, experiments were conducted on a scaled unipolar and bipolar lab setup to confirm the observations of the mathematical calculation and simulations.

Acknowledgements

The authors would like to thank VITO for the support in performing this research. This work has been supported by VLAIO in the Flux50 project BIDC (HBC.2018.0528).

References

[1] D. Wang, A. Emhemed, G. Burt, and P. Norman, "Fault analysis of an active LVDC distribution network for utility applications," in *2016 51st International Universities Power Engineering Conference (UPEC)*, 2016, pp. 1–6.

[2] L. Mackay, T. Hailu, L. Ramirez-Elizondo, and P. Bauer, "Towards a DC distribution system - opportunities and challenges," in *2015 IEEE First International Conference on DC Microgrids (ICDCM)*, 2015, pp. 215–220.

[3] G. Van Den Broeck, "Voltage control of bipolar dc distribution systems," Leuven, 2019. [Online]. Available: https://lirias.kuleuven.be/handle/123456789/643122

[4] G. Van den Broeck, T. Mai, and J. Driesen, "MatLVDC: A new open source Matlab toolbox to simulate DC networks including power electronic converters and distributed energy resources," in *2015 IEEE Power Energy Society General Meeting*, 2015, pp. 1–5.

[5] A. Agustoni, E. Borioli, M. Brenna, G. Simioli, E. Tironi, and G. Ubezio, "LV DC distribution network with distributed energy resources: analysis of possible structures," *IET Conference Proceedings*, pp. v5:10–v5:10(1), January 2005.

[6] H. Kakigano, Y. Miura, and T. Ise, "Low-Voltage Bipolar-Type DC Microgrid for Super High Quality Distribution," *IEEE Transactions on Power Electronics*, vol. 25, no. 12, pp. 3066–3075, 2010.

[7] P. Salonen, T. Kaipia, P. Nuutinen, P. Peltoniemi, and J. Partanen, "Fault analysis of LVDC distribution system," *in WESC*, 2008.

[8] A. A. S. Emhemed, K. Fong, S. Fletcher, and G. M. Burt, "Validation of Fast and Selective Protection Scheme for an LVDC Distribution Network," *IEEE Transactions on Power Delivery*, vol. 32, no. 3, pp. 1432–1440, 2017.

[9] X. Feng, L. Qi, and J. Pan, "A novel fault location method and algorithm for DC distribution protection," *IEEE Transactions on Industry Applications*, vol. 53, no. 3, pp. 1834–1840, 2017.

[10] S. D. Fletcher, P. J. Norman, K. Fong, S. J. Galloway, and G. M. Burt, "High-speed differential protection for smart DC distribution systems," *IEEE Transactions on Smart Grid*, vol. 5, no. 5, pp. 2610–2617, 2014.

[11] D. Wang, A. Emhemed, and G. Burt, "A novel protection scheme for an LVDC distribution network with reduced fault levels," in *2017 IEEE Second International Conference on DC Microgrids (ICDCM)*, 06 2017, pp. 69–75.

[12] S. Xue, C. Chen, Y. Jin, Y. Li, B. Li, and Y. Wang, "Protection for DC distribution system with distributed generator," *Journal of Applied Mathematics*, vol. 2014, 2014.

[13] K. C. Lee, A. Ukil, and Y. Yeap, "Short-circuit protection for MV LVDC grid," in *2014 IEEE PES Asia-Pacific Power and Energy Engineering Conference (APPEEC)*, 2014, pp. 1–6.

[14] J. Kaiser, K. Gosses, L. Ott, Y. Han, B. Wunder, M. März, F. Schork, K. Bühler, and T. Böhm, "Safety considerations for the operation of bipolar DC-grids," in *2017 IEEE International Telecommunications Energy Conference (INTELEC)*, 2017, pp. 327–334.

[15] C. Li, P. Rakhra, P. Norman, G. Burt, and P. Clarkson, "Metrology requirements of state-of-the-art protection schemes for DC microgrids," *The Journal of Engineering*, vol. 2018, no. 15, pp. 987–992, 2018.

[16] S. Ravyts, G. V. d. Broeck, L. Hallemans, M. D. Vecchia, and J. Driesen, "Fuse-based short-circuit protection of converter controlled low-voltage DC grids," *IEEE Transactions on Power Electronics*, vol. 35, no. 11, pp. 11 694–11 706, 2020.